

Magnetic Tunnel Junction—Metals and Semiconductors

Janusz Nowak, Chairman

Low resistance spin-dependent tunnel junctions with ZrAlO_x barriers

Jianguo Wang^{a)} and P. P. Freitas

Instituto de Engenharia de Sistemas e Computadores (INESC), R. Alves Redol 9-1, 1000-029 Lisbon and Department of Physics, Instituto Superior Tecnico (IST), Avenue Rovisco Pais, 1096 Lisbon, Portugal

E. Snoeck

Centre d'Elaboration de Matériaux et d'Etudes Structurales (CEMES-CNRS), BP 4347, F-31055 Toulouse Cedex, France

X. Battle and J. Cuadra

Departamento Fisica Fundamental, Universitat de Barcelona, Catalonia, Spain

Spin-dependent tunnel junctions with ZrAlO_x barriers were fabricated with low resistance \times area product $4 \Omega \times \mu\text{m}^2$, and tunnel magnetoresistance of 15.2%. Barrier fabrication was done by natural oxidation (5 min, at oxidation pressures ranging from 0.5 to 10 Torr). The junctions were deposited on top of 600 Å thick, ion beam smoothed, low resistance, Al electrodes. X-ray photoelectron spectroscopy analysis indicates the presence of AlO_x , ZrO_2 , some remnant metallic Zr, but no metallic Al in the as-deposited barriers. High resolution transmission electron microscopy indicates that ZrAlO_x forms an amorphous barrier that is smoother than pure crystalline ZrO_x or pure amorphous AlO_x barriers. These low resistance tunnel junctions are attractive for read head applications above 100 Gbit/in² where competitive signal to noise ratios imply resistance \times area product below a few $\Omega \times \mu\text{m}^2$, and tunneling magnetoresonance signals near or above 20%. © 2002 American Institute of Physics. [DOI: 10.1063/1.1447195]

I. INTRODUCTION

Low resistance spin-dependent tunnel junctions are possible candidates for replacement of spin valve sensors in read heads as recording densities move beyond 100 Gbit/in². As a current perpendicular to the plane sensor, the tunnel junction can be inserted directly in between the shields, avoiding the insulating layers¹⁻⁴ and improving linear density. For proper signal to noise ratio, and for compatibility with head preamps, tunnel junctions must have very low resistance (few $\Omega \times \mu\text{m}^2$) and maintain tunneling magnetoresonance (TMR) values near or excess than 20%. Results from various groups on low resistance junctions using naturally oxidized AlO_x barriers (5–7 Å Al) report resistance \times area ($R \times A$) products ranging from 5 to 20 $\Omega \times \mu\text{m}^2$, but with TMR values scaled down to 10%–20%.¹⁻⁶ Better control of oxidation time and pressure can further optimize these values.⁷ Another approach to produce low resistance junctions is to use lower band gap oxides (ZrO_x , HfO_x , among others) as barrier. ZrO_x , for example, is found to form polycrystalline barriers, with reasonable TMR values ($\approx 20\%$).⁸ The polycrystalline nature of the barrier may be detrimental for producing homogeneous ultrathin barriers due to the different oxidation speeds across grain boundaries. This article describes the properties of ZrAlO_x junctions prepared by natural oxidation.

Low resistance ($4-8 \Omega \times \mu\text{m}^2$, for 7 Å thickness), amorphous, ZrAlO_x barriers, with TMR values reaching 15.2% are obtained.

II. EXPERIMENT

The junctions used in this work have a bottom-pinned structure, glass / bottom lead / Ta 70 Å / NiFe 70 Å / MnIr 80 Å / CoFe 35 Å / ($\text{Zr}_{11}\text{Al}_{12}$) + Ox. / CoFe 35 Å / NiFe 40 Å / Ta 30 Å / TiW(N) 150 Å / top lead. Here NiFe, CoFe, and MnIr stand for $\text{Ni}_{81}\text{Fe}_{19}$, $\text{Co}_{90}\text{Fe}_{10}$, and $\text{Mn}_{83}\text{Ir}_{17}$, respectively. Except for the bottom and top leads, and the $\text{Ti}_{10}\text{W}_{90}$ (N) antireflective coating (ARC), all layers were deposited in a Nordiko 2000 magnetron sputtering system, with a base pressure of 5×10^{-8} Torr. During deposition, a magnetic field of 20 Oe was applied to induce parallel easy axis in the bottom and top magnetic layers. The ZrAlO_x is grown by depositing sequentially Zr (2.5–3 Å) and Al (4.5 Å), followed by natural oxidation (5 min at 0.5, 1, and 10 Torr). Bottom and top leads, and the ARC layer were deposited by magnetron sputtering in a Nordiko 7000 cluster system (base pressure 5×10^{-9} Torr). The bottom lead is formed by 600 Å of Al 1%Si 0.5%Cu (0.6 Ω/sq), subject to a postdeposition anneal at 400 °C for 30 min. The AlSiCu layer is then ion beam smoothed for 90 s at a substrate pan of 40°, leading to an atomic force microscope (AFM) rms roughness down to $< 2 \text{ \AA}$ ⁹ (rms around 10 Å before smoothed). The μm -size junctions were patterned by a self-aligned microfabrication

^{a)}Electronic mail: jianguo.wang@inesc.pt

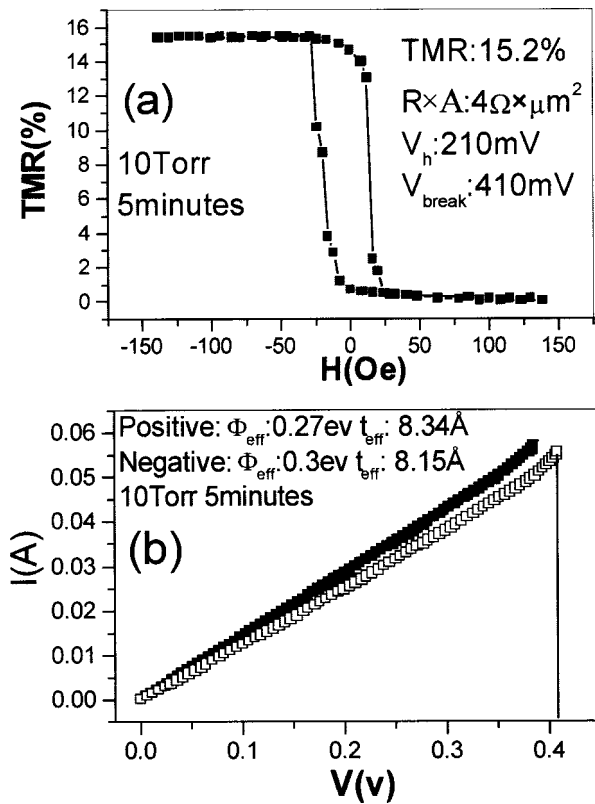


FIG. 1. (a) TMR minor loop, and junction parameters for a (Zr 2.5 Å/Al 4.5 Å) O_x junction after anneal at 240 °C for 40 min. (b) I - V curves and barrier parameters for both positive and negative bias voltage branches.

process using direct-write laser-lithography and ion-beam milling. Junctions were measured using a four-probe dc method. Anneals were carried out in a vacuum furnace (10^{-6} Torr) under a 3000 Oe magnetic field for 40 min, with ramp-up and cooldown times of about 1 h. X-ray photoelectron analysis (XPS) analysis was made in specially fabricated specimens allowing the separation of the different peaks requiring study (Zr, Al, Co, Fe, and their oxides in barrier region). Since the XPS signal comes from an area within a distance of about $2\lambda-3\lambda$ (λ is the inelastic mean free path for electrons) from the sample surface, low-energy ion beam (4 keV, 45°) etch was carried out to obtain a depth profile. The etch rate is around 6–10 nm/min, and each step takes 6 s. The structural characterization of the junctions was made by transmission electron microscopy (TEM) on cross sectional specimens. The specimens were glued face to face, mechanically polished, then ion milled to achieve electron transparency. The TEM experiments were carried out on a Philips CM30 microscope whose point resolution is 0.19 nm.

III. RESULTS AND DISCUSSION

Figure 1(a) shows the minor TMR loop of a ZrAlO $_x$ junction, where the barrier was formed by natural oxidation (10 Torr 5 min) of a (2.5 Å Zr/4.5 Å Al) film. The junction area is $1\mu m^2$. TMR of 15.2% and a resistance \times area product of $4\Omega\times\mu m^2$ are obtained. Due to the low resistance of the bottom lead compared with junction resistance, no current inhomogeneity across the junction area occurs. Junctions

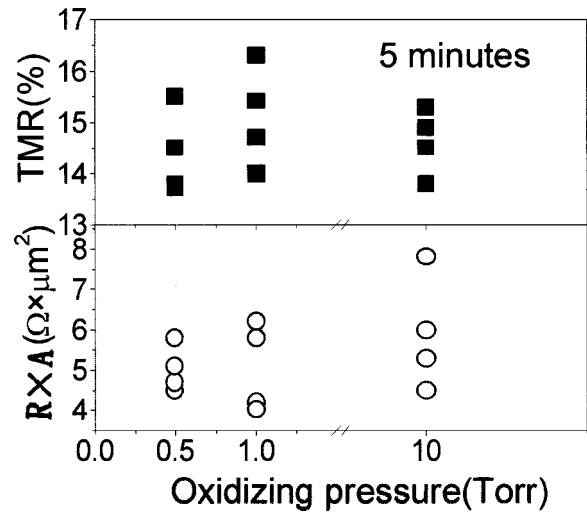


FIG. 2. (a) TMR dependence on oxidation pressure for (Zr 2.5 Å/Al 4.5 Å) O_x barrier junction. (b) Resistance \times area product dependence on oxidation pressure for (Zr 2.5 Å/Al 4.5 Å) O_x barrier junction.

were annealed at 240 °C for 40 min to set up the exchange bias field in the MnIr/CoFe bilayer.¹⁰ Figure 1(b) shows the current–voltage (I - V) curve measured up to 400 mV for both positive (current flow from top to bottom) and negative (current flow from bottom to top) bias voltages. After fitting the I - V curves by Simmon's model,¹¹ the effective barrier height and effective barrier thickness are 0.3 eV and 8.15 Å

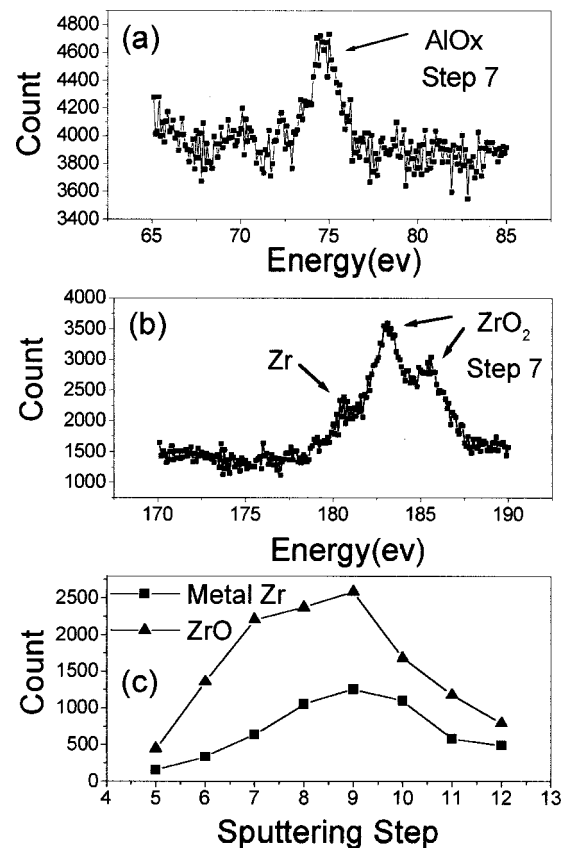


FIG. 3. XPS spectra (a) AlO $_x$, (b) Zr and ZrO $_2$, and (c) depth profile for Zr and ZrO $_2$ in the barrier region.

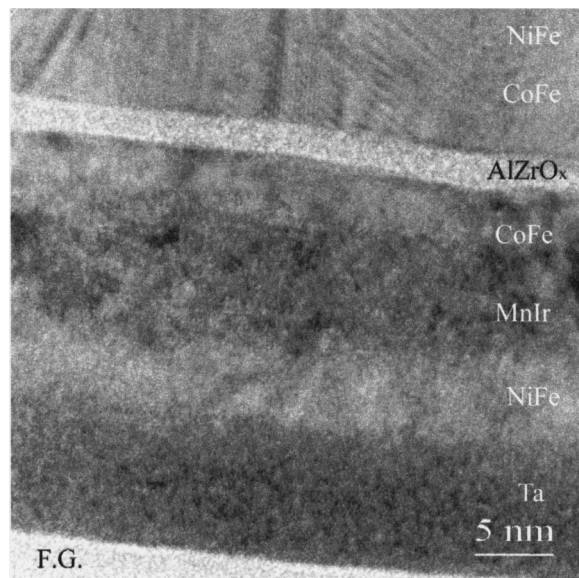


FIG. 4. HRTEM micrograph showing the stacking sequence of the junction and the low roughness of the amorphous ZrAlO_x barrier.

for the negative voltage branch, and 0.27 eV and 8.34 Å for the positive voltage branch, respectively. The small asymmetry observed for positive and negative bias voltages probably reflects incomplete oxidation of the Zr–Al film and nonhomogeneous oxidation profile at these short oxidation times required to provide low resistances, leading to different barrier properties at both interfaces. The bias voltage where the TMR signal drops to half its zero-bias value is 210 mV. Junction breakdown voltage is 0.412 V, measured in $1 \mu\text{m}^2$ junctions. The 15.2% TMR value is still low in comparison with that obtained in fully oxidized higher resistance AlO_x barriers (30% TMR for $R \times A > 40\text{--}70 \Omega \times \mu\text{m}^2$), but comparable to that observed in our lowest resistance AlO_x barriers ($12 \Omega \times \mu\text{m}^2$, 17% TMR, 7 Å Al, oxidized 5 min at 500 mTorr),⁷ but the resistance \times area product of the ZrAlO_x barriers is significantly lower. The low resistance values could also be associated with the expected lower band gap of the ZrAlO_x or part of the Zr left unoxidized.

Figure 2 shows TMR(a) and $R \times A$ (b) data obtained for a similar structure (junctions with $(2.5 \text{ Å Zr} + 4.5 \text{ Å Al})\text{O}_x$ as barrier) oxidized 5 min at different oxidation pressures (0.5, 1, and 10 Torr). These junction were annealed at 240 °C for 40 min. As can be seen, there is no major difference in the presented results (resistance is around $5 \Omega \times \mu\text{m}^2$, and with the TMR around 14%–15%), indicating that the same oxidation state is obtained in the three cases. This indicates that a fast oxidation mechanism is present in the three cases, namely the oxidation of the metallic layers (Zr+Al) controlled by the interface reaction rate between the formed oxide surface and the bulk gas.

In order to clarify the oxidation status of the barrier, an XPS analysis was performed in specially prepared samples, allowing the observation of the different oxide peaks. Figure 3 shows data obtained in the structure, $\text{Si/Ti}50 \text{ Å} / \text{CoFe}35 \text{ Å} / (2.5 \text{ Å Zr} + 4.5 \text{ Å Al})\text{O}_x / \text{CoFe}35 \text{ Å} / \text{Ti}50 \text{ Å}$. The barrier was oxidized 5 min at 10 Torr. Figure 3(a) shows the XPS

spectra for AlO_x , and Fig. 3(b) for metallic Zr and ZrO_2 . The data were taken in the barrier region (step 7). For Al, all the signals are AlO_x . The peak is symmetric and appears at 74.7 eV, as expected for aluminum oxide. No metallic Al is found. On the contrary, Fig. 3(b) shows that evidence is found for metallic Zr left unoxidized in the barrier. The metallic contribution should appear at 179 eV ($3d5/2$) and 181.5 ($3d3/2$), while ZrO_2 should appear at 182–182.5 ($3d5/2$) and 184.5–185 ($3d3/2$). The amount of metallic Zr left over in the barrier is estimated at 13%. Figure 3(c) shows the depth profile obtained for metallic Zr and ZrO_2 in the barrier. Notice that the amount of metallic Zr increases near the junction bottom, as expected.

High resolution transmission electron microscopy (HRTEM) was used to characterize the barrier. For this study, junction structure was, glass/Ta70 Å / NiFe70 Å / MnIr 80 Å / CoFe 35 Å / $(4.5 \text{ Å Zr} + 4.5 \text{ Å Al})\text{O}_x$ / CoFe 35 Å / NiFe 40 Å / Ta 30 Å. For these thicker barriers, radio frequency (rf) plasma oxidation was used (40 in., 35 W rf, 5 mTorr O_2). The HRTEM micrograph in Fig. 4 in which the stacking sequence: float Glass / Ta / NiFe / MnIr / CoFe / ZrAlO_x / CoFe / NiFe clearly shows up. The ZrAlO_x oxide layers is 2.5 nm thick at the as-deposited state and appears to be amorphous with smooth top and bottom interfaces. The same experiments performed on the ZrO_x barriers and AlO_x barriers reveal that the ZrO_x oxide layer is crystalline while the AlO_x insulating layer was found to be amorphous. It is therefore concluded that the addition of Zr favors the wetting of the bottom CoFe electrode by the oxide and that the 50% Al/Zr ratio is sufficient to keep the oxide amorphous.

IV. CONCLUSION

In conclusion, low resistance tunnel junctions with ZrAlO_x barriers have been successfully fabricated. The inclusion of Zr has helped to provide smoother interfaces and form homogeneous barriers. Low resistance is due either to leftover metallic Zr in the barrier, or the expected lower band gap of ZrAlO_x .

ACKNOWLEDGMENTS

This work was supported by the PRAXIS projects PCEX/C/FIS/28/96 and P/CTM/10220/1998. J.W. acknowledges the support of a PRAXIS/BD/15572/98 Ph.D Grant.

¹K. Shimazawa *et al.*, IEEE Trans. Magn. **36**, 2542 (2000).

²D. Song, J. Nowak, R. Larson, P. Kolbo, and R. Chellew, IEEE Trans. Magn. **36**, 2545 (2000).

³K. Ohashi *et al.*, IEEE Trans. Magn. **36**, 2549 (2000).

⁴P. P. Freitas, S. Cardoso, R. C. Sousa, W. Ku, R. Ferreira, V. Chu, and J. P. Conde, IEEE Trans. Magn. **36**, 2796 (2000).

⁵J. J. Sun, N. Kasahara, K. Sato, K. Shimazawa, S. Araki, and M. Matsuzaki, J. Appl. Phys. **89**, 6653 (2001).

⁶J. R. Childress, M. M. Schwickert, R. A. Fontana, M. Ho, and B. A. Gurney, J. Appl. Phys. **89**, 7353 (2001).

⁷Z. G. Zhang, P. P. Freitas, A. R. Ramos, N. P. Barradas, and J. C. Soares, Appl. Phys. Lett. **79**, 2219 (2001).

⁸J. Wang, P. P. Freitas, E. Snoeck, J. C. Soares, Appl. Phys. Lett. (in press).

⁹S. Cardoso, Z. G. Zhang, P. P. Freitas, P. Wei, N. Barradas, and J. C. Soares, J. Appl. Phys. **89**, 6650 (2001).

¹⁰H. Li, P. P. Freitas, Z. Wang, J. B. Sousa, P. Gogol, and J. Chapman, J. Appl. Phys. **89**, 6904 (2001).

¹¹J. G. Simmons, J. Appl. Phys. **34**, 1793 (1963).